



HAL
open science

Dependence of elastic properties of argillaceous rocks on moisture content investigated with optical full-field strain measurement techniques

Diansen Yang, Michel Bornert, Serge Chanchole, Hakim Gharbi, Pierre Valli, Behrouz Gatmiri

► To cite this version:

Diansen Yang, Michel Bornert, Serge Chanchole, Hakim Gharbi, Pierre Valli, et al.. Dependence of elastic properties of argillaceous rocks on moisture content investigated with optical full-field strain measurement techniques. *International Journal of Rock Mechanics and Mining Sciences*, 2012, 53, pp.45-55. 10.1016/j.ijrmms.2012.04.004 . hal-00717140

HAL Id: hal-00717140

<https://enpc.hal.science/hal-00717140>

Submitted on 25 Apr 2022

HAL is a multi-disciplinary open access archive for the deposit and dissemination of scientific research documents, whether they are published or not. The documents may come from teaching and research institutions in France or abroad, or from public or private research centers.

L'archive ouverte pluridisciplinaire **HAL**, est destinée au dépôt et à la diffusion de documents scientifiques de niveau recherche, publiés ou non, émanant des établissements d'enseignement et de recherche français ou étrangers, des laboratoires publics ou privés.



Distributed under a Creative Commons Attribution - NonCommercial 4.0 International License

Dependence of elastic properties of argillaceous rocks on moisture content investigated with optical full-field strain measurement techniques

D.S. Yang^{a,*}, M. Bornert^b, S. Chanchole^a, H. Gharbi^a, P. Valli^a, B. Gatmiri^c

^a Laboratoire de Mécanique des Solides, Ecole Polytechnique, 91128 Palaiseau, France

^b Laboratoire Navier, Université Paris-Est, Ecole des Ponts ParisTech, Champs-sur-Marne, 77544 Marne-la-Vallée, France

^c Agence nationale pour la gestion des déchets radioactifs (ANDRA), 92298 Châtenay-Malabry, Cedex, France

The mechanical behaviour of the argillaceous rock considered in France as a potential host rock for nuclear waste repository strongly depends on water content. In order to quantify the dependence of the mechanical properties on humidity, an experimental setup that combines hydromechanical loadings with optical observations and digital image correlation (DIC) has been developed. It allows investigation of the hydromechanical behaviour of a material from the sample scale (cm) down to micrometric scale (100 μm). Using this system, the shrinkage and swelling properties of the argillaceous rock at various constant uniaxial stresses, and the linear mechanical behaviour of the material at different moisture levels, were experimentally studied. A quasi-linear relation between the relative humidity, ranging from 39% to 85%, and the deformation during dehydration and rehydration is found at both the sample scale (cm), and a mesoscopic scale of a few hundred micrometres. This relation depends on the applied stress with much less swelling at higher axial compressive stress. In addition, a linear decrease of the axial Young's modulus (normal to bedding plane) with an increase of the relative humidity is observed.

1. Introduction

Due to its very low permeability ($< 10^{-21} \text{ m}^2$), the Callovo-Oxfordian (COx) argillaceous formation of the Meuse/Haute Marne (MHM) site near Bure (eastern France) at a depth of about 500 m, is considered as a possible host rock for high level radioactive nuclear waste repository by ANDRA (Agence Nationale pour la Gestion des Déchets Radioactifs, the French agency for radioactive waste management) [1]. The construction of the underground nuclear waste repositories will strongly disturb the initial thermo-hydro-chemo-mechanical equilibrium of the site. In addition to direct mechanical perturbations during excavation, which induce redistribution of the stresses and potential damage of the surrounding rock mass, the ventilation of the galleries will also modify the moisture content of the rock, resulting in shrinking or swelling, and more generally modifying the physical-chemical properties of the material [2,3]. Safety concerns about preservation of confining properties of the rock mass at short and long time scales require a deep understanding of the hydromechanical behaviour of the host rock. In particular

the dependence of elastic and nonlinear (plasticity, damage, creep etc.) properties with moisture content needs to be quantified. In addition, in order to construct physically based micromechanical models of these dependencies, the various micromechanisms at their origin and their characteristic scales need to be identified.

The MHM argillite is a complex material composed of different minerals. It can be described as clay matrix (mostly illite and smectite) with embedded calcite and quartz grains and several other minerals in lower content [1,3,4]. Such a mineralogical composition leads to a complex behaviour at various scales when the material is subjected to hydromechanical loading. A high grain content may increase the overall rigidity of the material while a high smectite content induces large swelling and shrinkage strains which may degrade the material during hydration and dehydration. The heterogeneous mineralogical composition may induce a coupled hydric and mechanical behaviour during hydration.

Many studies on the hydromechanical behaviour of the COx argillite have been carried out at the macroscale (cm) [5–11]. Some of them focus on the dependence of the elastic properties with moisture level [7,11] and while others have concentrated on the shrinkage and swelling induced by suction variation [8–9]. In order to further study the hydromechanical behaviour of the COx argillite and identify its micro-mechanisms, much effort has been devoted to developing a specific optical setup to characterize the low strain levels, typically below 10^{-3} , generated by

* Corresponding author.

E-mail addresses: yang@lms.polytechnique.fr (D.S. Yang), michel.bornert@enpc.fr (M. Bornert).

moisture and mechanical load, both at the macroscopic scale of a centimetric laboratory sample and at local scales (100 μm and below) [5,12]. The resolution in terms of strain measurements of this setup needs to be rather high: the creep stain rate of this material is less than $10^{-10}/\text{s}$, i.e. about 10^{-4} per week and the swelling/shrinking strain is about 10^{-4} per humidity degree. The swelling/shrinking depends on the composition, concentration and pressure of the pore-liquid, the stress state and the initial saturation of the material. Many studies were done on the swelling/shrinking of the COx argillite without applied stress [8–9], but there were only a few studies on the behaviour under combined moisture and mechanical loading. This paper will provide some new experimental results of the behaviour of the COx argillite subjected to coupled hydromechanical conditions obtained with the developed optical setup, which allows to simultaneously and independently control the moisture and apply the uniaxial stress, and to perform a real time continuous optical observation at both the sample scale (cm) and the local scale ($\sim 100 \mu\text{m}$).

We first briefly describe the experimental setup to monitor samples submitted to uniaxial compression under controlled moisture content with full-field optical measurement techniques and focus on several specific procedures to improve the optical measurement accuracy. The physical properties of the argillaceous rocks under investigation are presented in Section 3 while the sample preparation and loading conditions are given in Section 4. We present in Section 5 the experimental results on, first, the swelling and shrinkage properties at various uniaxial stresses and, second, the evolution of elastic properties with moisture content. These behaviours are investigated at various scales.

2. Experimental setup and measurements accuracy

2.1. Experimental equipments

The Digital Image Correlation (DIC) technique is widely used in solid mechanics to investigate the mechanical properties of structural materials [13–15] and has recently been applied to geomaterials at various scales, in 2 and 3 dimensions [13,16–18]. It consists in tracking the grey level distributions in subsets of images of a sample acquired by a CCD camera at different loading states to determine displacement and strain fields. In a previous study [4], this technique has been used to investigate at both sample scale (cm) and microscopic scale (100 μm) the mechanical response to uniaxial compression of a sample of COx rock preliminary brought to equilibrium with a prescribed relative humidity. This system has been extended to investigate the coupled hydromechanical behaviour of this rock. Its accuracy has been improved in order to measure the low strains (of the

order of 10^{-3}) induced by variations of moisture and the very low strains observed during creep (of the order of $10^{-4}/\text{week}$). The new experimental setup mainly consists of three parts: macroscopic and microscopic optical setups, mechanical loading device and suction control equipment (Fig. 1).

The macroscopic optical setup (referred to in the following as ‘MacroDIC’) uses a 16 Megapixels CCD camera, which is equipped with a macrolens (focal length $f=120 \text{ mm}$, aperture $F=1:5.6$). The chosen lens exhibits very low geometric distortion when the optical magnification equals one, as used in this study. The observed flat surface area is $24 \times 36 \text{ mm}^2$ and the pixel size is $7.4 \mu\text{m}$. The working distance is about 240 mm. Two groups of four blue (wavelength=440–490 nm) Light Emitting Diodes (LED) symmetrically and uniformly illuminate the flat surface of the sample with an incident angle of about 45° . The blue LEDs with shorter wavelength have been preferred to red, green or even white LEDs because they provide a larger depth of field (about 1 mm) for a given diffraction pattern size, the latter playing an important role in the optimisation of the setup as shown in Ref. [12]. In addition, blue light is close to the peak quantum efficiency of the sensor. The camera is mounted on a manual X–Y–Z translation stage with about $10 \mu\text{m}$ positioning accuracy. This macroscopic optical setup is held fixed during the whole hydro-mechanical loading history.

The microscopic optical setup (referred to as ‘MicroDIC’) makes use of a 4 Megapixels CCD camera and an infinity-corrected apochromatic $\times 10$ objective lens. With this optical combination, the observed object area is $1.5 \times 1.5 \text{ mm}^2$ and the pixel size is $0.74 \mu\text{m}$. The working distance is 34 mm. In consideration of the small depth of field of optical microscopy, about $3.5 \mu\text{m}$ in the present case, the camera has been mounted on a servo-controlled micrometric X–Y–Z translation stage. With this servo-control, the Z position (normal to sample surface) is automatically adjusted for sharp focus, by means of a contrast maximisation algorithm, and the camera can be moved automatically along X and Y directions to observe several juxtaposed zones and centre them, with an accuracy of about $3 \mu\text{m}$, on preliminary defined positions of interest by means of standard DIC algorithms. Both normal and lateral white illumination modes are used. An additional manual rotation stage is used to align the X–Y translation stage with the surface of the sample so that focus is kept when the microscope is moved all over the whole flat surface.

The MicroDIC setup is opposite to the MacroDIC setup but both are mounted on the same rigid optical table, which is itself mounted on a rigid electromechanical machine used to apply the axial force on the cylindrical sample. Both force and displacement control can be used. Teflon sheets are used to reduce friction effects at the sample/machine interface and moments are reduced by means of a spherical bearing.

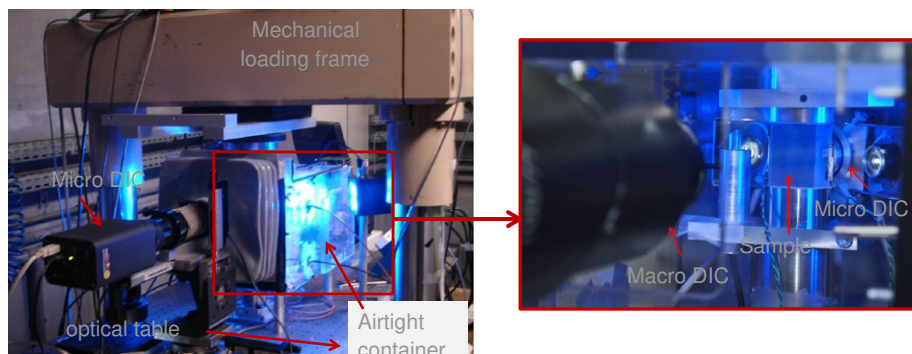


Fig. 1. Views of the setup designed to combine uniaxial compression test under controlled moisture content with optical multiscale full-field strain measurements.

Relative humidity is prescribed by means of supersaturated saline solutions which are placed near the sample inside an airtight transparent container, about $25 \times 25 \times 40$ cm in size, in which holes have been machined for the optics and the loading line. Two hygrometry sensors are placed inside the airtight container to record continuously the actual relative humidity near the sample, and a third one outside to record continuously the atmospheric humidity. Temperature is recorded as well. It has been observed during the test described in Section 4, that once the sample has reached equilibrium with the saline solution, there are still low amplitude fluctuations of the humidity inside the container which are correlated with the variations of the atmospheric humidity. This is due to imperfect tightness of the container, probably due to the holes for the optical and loading line which could not be perfectly sealed. Because of this imperfection, it was not possible to prescribe a relative humidity higher than 85%.

2.2. Two procedures to improve the measurements accuracy

As small elastic and shrinkage or swelling strains need be quantified, the DIC measurement accuracy needed to be improved. Several procedures have been developed for this purpose among which the two following ones are the most important [12]. The first one aims at precisely quantifying the actual so-called systematic DIC errors, i.e. the systematic under or overestimation of displacement components by DIC, correlated with the fractional part of the real displacement, expressed in pixels. More details on these errors, quantified by an “S-shaped” curve giving these errors as a function of the fractional part of the displacement, can be found in Refs. [19,20]. Their intensity depends on several factors such as available contrast, image quality, noise and chosen image correlation algorithm. It has been shown [12] that their amplitude can be reduced by, first, an appropriate choice of the lens aperture, which controls the size of diffraction patterns, and second, the selection of the best grey level interpolation scheme used by the DIC algorithm, so as to adapt them to the available natural contrast of the rock used as DIC patterns.

To do so, a simple and fast procedure to quantify the actual DIC systematic errors relative to the MacroDIC setup has been developed. It is based on a statistical analysis of the apparent deformation induced by a uniform out-of-plane motion of the sample with respect to the camera. While technical details can be found in Refs. [12,16], an illustrative result is given in Fig. 2a, where the systematic error associated with a bilinear grey-level interpolation, for the natural contrast of the argillaceous rock sample, is plotted for lens 5 apertures. The results show a strong dependence of this error with aperture both in terms of amplitude and shape of the S-shaped curve. In addition, a more than 10-fold reduction of these errors can be achieved when an optimal aperture is selected. The same analysis with a biquintic interpolation shows similar tendencies, but with different curves: optimal aperture is now between 2 and 3, but with small differences between apertures 2, 3 and 4 (Fig. 2b).

The second procedure aims at correcting the errors induced by the overall micrometric out-of-plane motion of the sample on the macroscopic DIC measurements. Due to several factors, such as Poisson’s effect, small amounts of specimen bending, etc. [21], global out-of-plane motions of the sample surface with respect to the camera are unavoidable. In addition, the loading device may move itself slightly with respect to an ideal setup, generating an overall out-of-plane motion of the sample. This is in particular the case on our setup where the loading device is not very rigid transversally because of the presence of the airtight container which requires a “long” loading system. These motions will

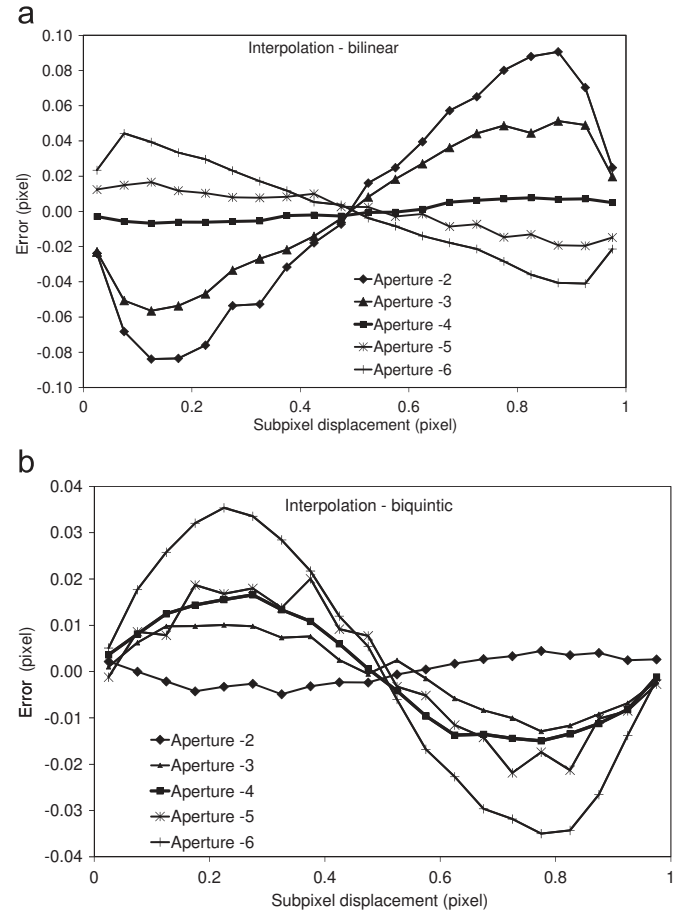


Fig. 2. Systematic errors curves for various lens apertures: DIC with bilinear interpolation (a) and biquintic interpolation (b).

induce a magnification variation on the MacroDIC images, which depend linearly on the out-of-plane motion. The overall out-of-plane shift is quantified by the MicroDIC setup and its already-described automatic focussing system to record the motion of the flat surface of the sample opposite the surface observed with the MacroDIC setup. As illustrated in Fig. 3, the relative displacement of the other side of the sample with respect to the fixed macroscopic lens can be evaluated with micrometric resolution by combining the measured motion dZ_{micro} and the transverse deformation of the sample, assumed to be macroscopically identical along the two transverse directions with respect to loading direction, and measured by DIC. With this displacement and the calibrated dependence of the MacroDIC magnification with out-of-plane motion, the apparent strain can be corrected. Such a correction is necessary to measure elastic moduli, as without them the measured (apparent) strains do not evolve linearly with applied stress [12,16].

With these improvements, the current optimised optical setup ensures an accuracy better than 10^{-5} at the sample scale (cm) and 10^{-4} at the micrometric scale (100 μm). It is noted that the strain of the global zone or of any selected local zone is determined using the method of averaging the deformation gradients over the domain of interest described in Ref. [22], which requires the knowledge of in-plane displacement on the boundaries of these zones only. More precisely, overall strains derived from the macroDIC setup are relative to the whole region of interest (22×32 mm² in size, see Fig. 14a) while strain maps obtained with macroDIC correspond to a local gauge length of 450 μm . Concerning MicroDIC (see Fig. 15a), overall data refer to areas of about 1.1×1.2 mm² in size, and local data presented in

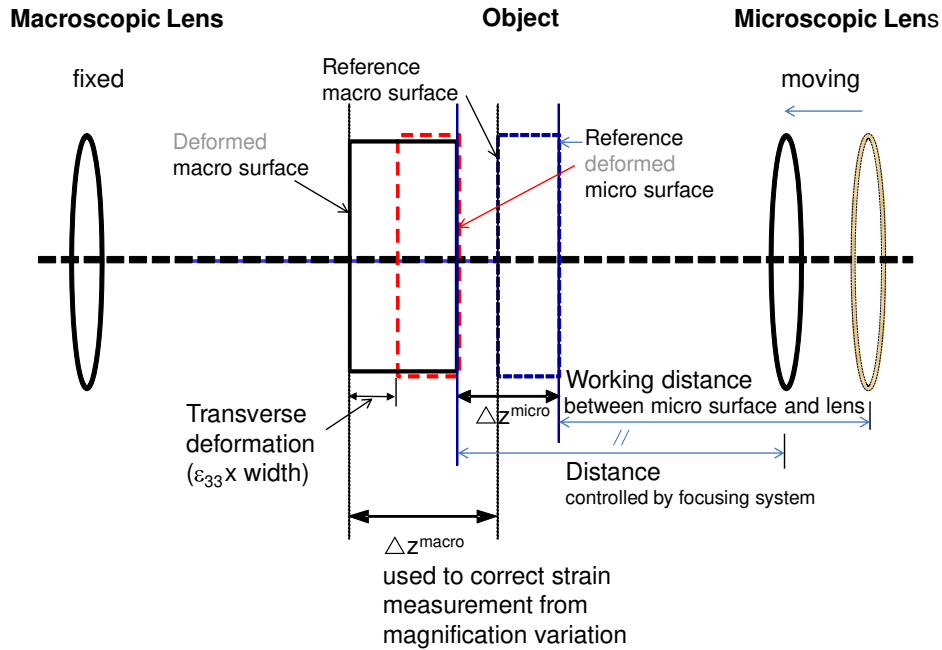


Fig. 3. Principle of the correction of the MacroDIC errors induced by the out-of-plane motion of the sample.

maps are computed for a gauge length of $90\ \mu\text{m}$. In addition, MicroDIC data have also been averaged on intermediate areas of a few $100\ \mu\text{m}$ in width. Note also that in the following measures of strain are positive in contraction.

3. Material

The COx argillaceous rock contains an average of 40%–45% clay minerals (mass percentage), 22%–37% carbonates, 25%–30% quartz and less than 5% other materials (for example, pyrite) [1,4]. A microscopic investigation by means of scanning electron microscopy (SEM) of the core plug EST05749 taken in MHM at 504.13 m depth, illustrated by the micrograph represented in Fig. 4 shows the various components of the studied material and their typical sizes, as well as several preexisting mesoscale cracks. The total porosity of the argillaceous rocks, evaluated by mercury injection porosimetry, varies between 12% and 18% and the pores are mainly mesopores (20–50 nm). Such a pore size distribution leads to a very low permeability ($\sim 10^{-22}\ \text{m}^2$) [23,24].

The initial water content of such argillaceous rocks in the as-received core plugs provided by ANDRA usually varies between 5% and 9% and the water is mainly held in the clayey matrix [4]. In this study, the initial water content of the core plug EST05749 is estimated to be 6.33%, as measured from 6 reference samples extracted from the same plug by drying them in an oven at $105\ ^\circ\text{C}$. The ultrasound velocity is measured on the same samples in the initial state to be about $2630\ \text{m/s}$. The apparent density of the samples is evaluated at $2.4\ \text{g/cm}^3$.

Several cylindrical samples have been taken from this core plug with a diameter of $36\ \text{mm}$ and a height of about $36\ \text{mm}$. Their axis is perpendicular to the stratification plane. One sample has been first freely dehydrated and rehydrated by the suction control technique [8,25] in the airtight container, where the relative humidity was controlled using supersaturated saline solutions. The relative humidity varied between 50% and 98%. The sample weight has been continuously recorded during the test. About ten days were needed to reach the moisture equilibrium at each step of the hydration/dehydration cycle. The obtained sorption and desorption curve, represented in Fig. 5, is

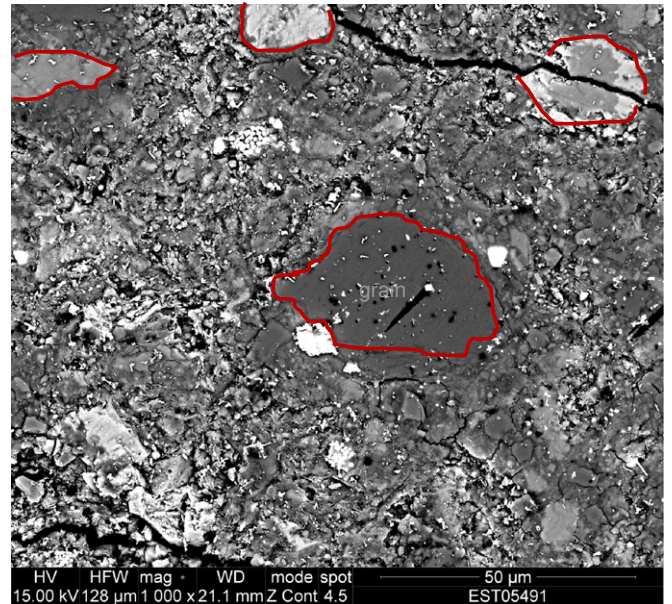


Fig. 4. Microstructure of the core plug EST05749.

close to that obtained by Pham et al. [8], except for high relative humidity. According to the almost linear relation between water content and relative humidity observed for our material, the sample at the initial state (i.e. at the beginning of the sample preparation) can be estimated to be in equilibrium with a relative humidity of 87%. A similar sample was chosen for the hydro-mechanical test presented in next sections.

4. Experimental procedure

4.1. Surface preparation

Two symmetric flat surfaces in diametral opposition were machined on the sample, one facing the macroscopic camera

and the other facing the microscopic camera. The width of these flat surfaces is about 24 mm so as to adapt them to the MacroDIC field of view, so that the remaining thickness of the sample between the two flat surfaces is 27 mm. Given the very small depth of field of the optical microscope, the two flat surfaces were then gradually polished from grade 800 to 4000 using abrasive paper. The latter grade corresponds to a grain size of 5 μm [9].

After sample preparation, several cracks were found, most of them parallel to the stratification plane (Figs. 14a and 15a). They were considered, according to earlier results [5], to be areas of interest, with specific responses to the moisture and mechanical loads. A local zone ($1.1 \times 1.2 \text{ mm}^2$) with a transverse crack crossing the whole field of view (Fig. 15a) and another local zone of same size, without visible crack but with an inhomogeneous mineralogical composition revealed by the grey level fluctuations at millimetric scale (Fig. 15b), have been selected as regions of interest for the 'MicroDIC' observations during the coupled hydromechanical test.

4.2. Loading paths

The prepared sample was then placed in the airtight container. A load of 0.7 kN, corresponding to 1 MPa, was firstly applied on the ends of the sample by controlling the displacement rate at 1 $\mu\text{m/s}$. The sample was then dehydrated with a controlled environmental humidity (60%) less than the initial humidity of the sample (about 87%). When the sample reached the moisture equilibrium (after about 2 weeks), two cycles of mechanical loading and unloading (uniaxial stress σ varying between 1 and 8 MPa) were prescribed to determine the mechanical elastic properties at this moisture content. More precisely, the sample was first loaded at the same displacement rate as above (corresponding to a deformation rate of about $3 \times 10^{-5} \text{ s}^{-1}$), for about 10 min; the stress was then kept constant for about 15 min until stabilisation of the deformation of the sample; it was then

unloaded at the same rate and again kept at a constant stress of 2 MPa until stabilisation; the whole cycle was then reproduced a second time. The whole mechanical loading procedure lasted about 2 h. Then, the axial stress was again kept constant (at 2 MPa) for the next dehydration or rehydration test, with a similar evaluation of elastic properties at the end. In this study, four saline solutions ($\text{CaCl}_2 \cdot 6\text{H}_2\text{O}$, NaNO_2 , NH_4Cl , $\text{CuSO}_4 \cdot 5\text{H}_2\text{O}$) were used to cover a large range of relative humidity during the hydration and dehydration cycles. They theoretically correspond to relative humidities of 36%, 66%, 79%, 98% respectively.

To study the influence of the applied stress on swelling and shrinking of the COx argillite, three cycles of rehydration and dehydration were performed at 2, 8.5 and 0.3 MPa, respectively. The cycles of mechanical loading and unloading were performed at each moisture equilibrium state. Finally, 16 hydration or dehydration stages and 16 mechanical loading/unloading tests were performed on the same sample as summarized in Fig. 6.

In fact, the actual loading path and the test time differed slightly from this ideal presentation. First, after the third elastic test, the stress was increased to 2 MPa during the hydration stages. Second, during the cycle of mechanical loading at the relative humidity of 85%, the axial stress was only increased to 6 MPa to avoid any plastic strain, expected to develop at lower stresses for higher moisture content. Third, because of the limits of the container sealing conditions, the measured moisture levels in the container deviated somewhat from the theoretical ones presented above and the real humidity varied between 39% and 85%. In order to improve the sealing conditions, the first cycle of dehydration and rehydration at 1 or 2 MPa was kept relatively long (6 months) and the whole test lasted 9 months. The actual moisture and stress loading path is shown in Fig. 7, together with the axial strain curves at macroscale (cm) measured by MacroDIC. Note that the temperature turned out to be rather constant with limited long term fluctuations (maximal amplitude below 4 $^\circ\text{C}$) due to the heating system of the building, and in general much

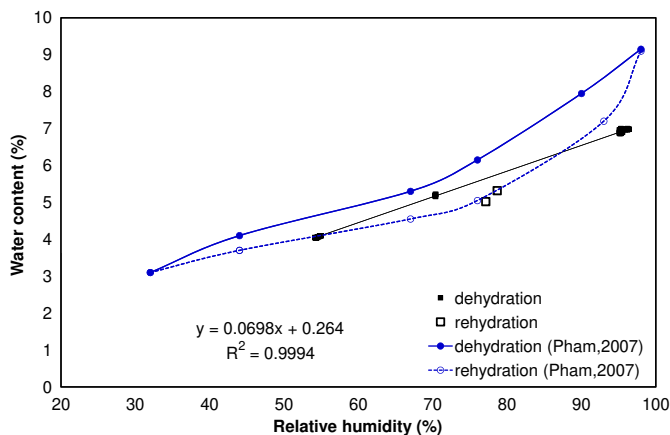


Fig. 5. Sorption curve of the COx argillite.

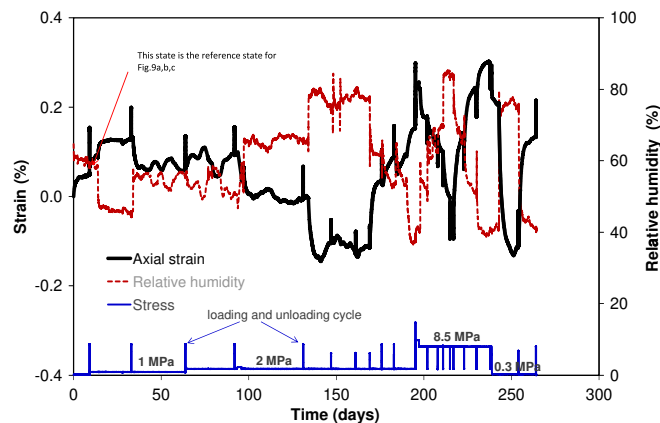


Fig. 7. Applied stress, macroscopic axial strain and measured relative humidity versus time for the whole experiment.

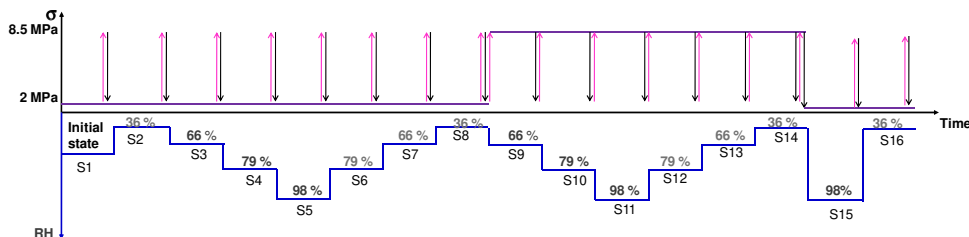


Fig. 6. Illustration of the planned moisture-mechanical loading path.

lower short term fluctuation during a given hydration stage (0.5 °C).

During the mechanical loading, the MacroDIC camera recorded one image every three seconds and the MicroDIC scanned four zones of interest, among which the two representative zones mentioned above and presented in Fig. 15a and b, at a rate of 5 s per image (including the positioning and focussing procedures). During the dehydration and rehydration tests, the MacroDIC and the MicroDIC continuously captured one image per 30 min during the first day and per hour during the following days until the moisture equilibrium state was reached. Hundred thousands of images, 32 Mbytes in size for MacroDIC (Fig. 14a) and 8 Mbytes in size for MicroDIC (Fig. 15a and b), were processed with the Unix-based in-house DIC software CMV, developed at LMS and Navier. The average strain over different zones (Figs. 14 and 15) and the full-field strain are obtained. Note that the chosen subset size is 30 pixels=225 μm for the macroDIC image analysis (Fig. 14a), with 146 \times 96 measurement positions, and 60 pixels=45 μm for the MicroDIC analysis, with 16 \times 18 positions (Fig. 15). More classical measurements (LVDT placed between two ends of the pistons which were in contact with the ends of the sample, three strain gauges glued on the sides of the sample at mid height: two longitudinal and one transversal. Data presented in Section 5 are those measured with longitudinal one which gave very similar results with those of the other one) at macro-scale (cm) were also recorded during the test.

5. Results and discussion

The measurements of the shrinkage and swelling properties and the elastic mechanical response at different moisture contents of the argillite are now summarised.

5.1. Shrinkage and swelling of the argillaceous rocks

Due to many physical and chemical mechanisms, such as the chemical reaction between smectite and water leading to crystal-line swelling, the physical reaction (hydration of exchangeable cations, attraction by osmosis, etc.), and the mechanical dilatation–contraction induced by the capillary pressure, etc. [25–29], the argillaceous rocks dilate during rehydration and contract during dehydration. The axial strain curve obtained at the macroscopic scale (cm) by MacroDIC shows evidence of the shrinkage and swelling properties of the argillite during the dehydration and rehydration cycles (Fig. 8a). The axial strains obtained at various scales (100 μm –cm) as function of time during rehydration at 2 MPa (Fig. 8a) and during dehydration at 8.5 MPa (Fig. 8b) illustrate that the sample required more than one week to reach the equilibrium when the relative humidity was kept constant. This long equilibrium time is related to the very low permeability of the material [8,24]. As an example of result, the permanent axial strain at the macroscopic scale during dehydration at 8.5 MPa when the humidity decreased from 52% to 39% is about 0.1% (see Fig. 8b, note that the initial RH peak at over 60% in this plot is induced by the opening of the container to replace the saline solutions).

All the measurements obtained by different methods (LVDT, gauge strain, MacroDIC and MicroDIC averaged over a 180 \times 180 μm^2 zone) and reported in Fig. 8 are consistent. The MacroDIC strain measurements determined from the whole surface (22 \times 32 mm^2) are slightly lower than those measured by LVDT, which is an indirect measurement which includes an additional strain related to the deformation of the Teflon sheet between the pistons and the ends of the sample. The small difference between the MacroDIC strain and the MicroDIC strain

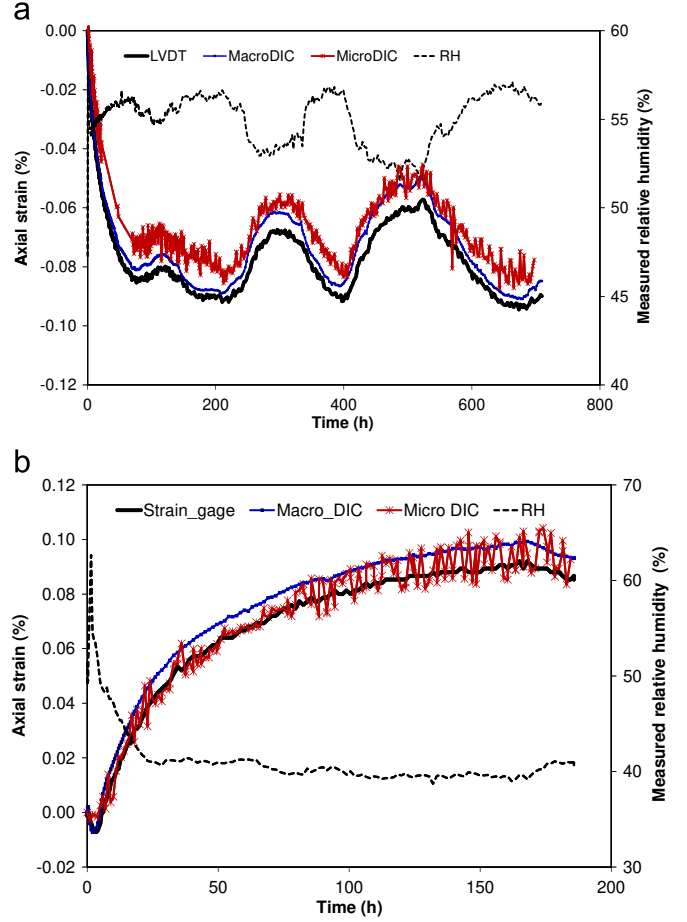


Fig. 8. Axial strain curve at various scales during rehydration (RH from 45% to 58%) at 2 MPa (a) and during dehydration (RH from 60% to 40%) at 8.5 MPa (b).

determined from the considered local zone is likely to be related to the structural and mineralogical heterogeneity. The values of the strain gauge are slightly lower than those of the MacroDIC strain in Fig. 8b. As the difference of the strain measurements between the traditional methods and the optical methods at macroscale are small, only the optical results will be presented in the following.

Fig. 9a and b report the MacroDIC axial and transverse strains of the sample in equilibrium with various relative humidity, considering the equilibrium state under the relative humidity of 60% and 1 MPa stress as the reference state. A quasi-linear relation between these equilibrium strains and the relative humidity during rehydration and dehydration at constant stresses is found in both the axial direction (Fig. 9a) and the lateral direction (Fig. 9b). Moreover, this quasi-linear relation is reversible during the cycle of hydration and dehydration at low axial stress (0.3 MPa and 2 MPa). This relation can be expressed as

$$\varepsilon_{\text{axial}} = -0.0091 \times RH + 0.5374 \text{ at 2 MPa, RH in \%, } \varepsilon \text{ in \%} \quad (1)$$

However, it is irreversible during the cycle of dehydration and rehydration at 8.5 MPa (Fig. 9). The sample swelled during rehydration less than at 2 MPa, and it contracted during dehydration very slightly more than at 2 MPa. The relations between the permanent axial strain and the relative humidity can be formulated as

$$\varepsilon_{\text{axial}} = -0.0053 \times RH + 0.5133 \text{ during rehydration at 8.5 MPa} \quad (2)$$

$$\varepsilon_{\text{axial}} = -0.0094 \times RH + 0.8739 \text{ during dehydration at 8.5 MPa} \quad (3)$$

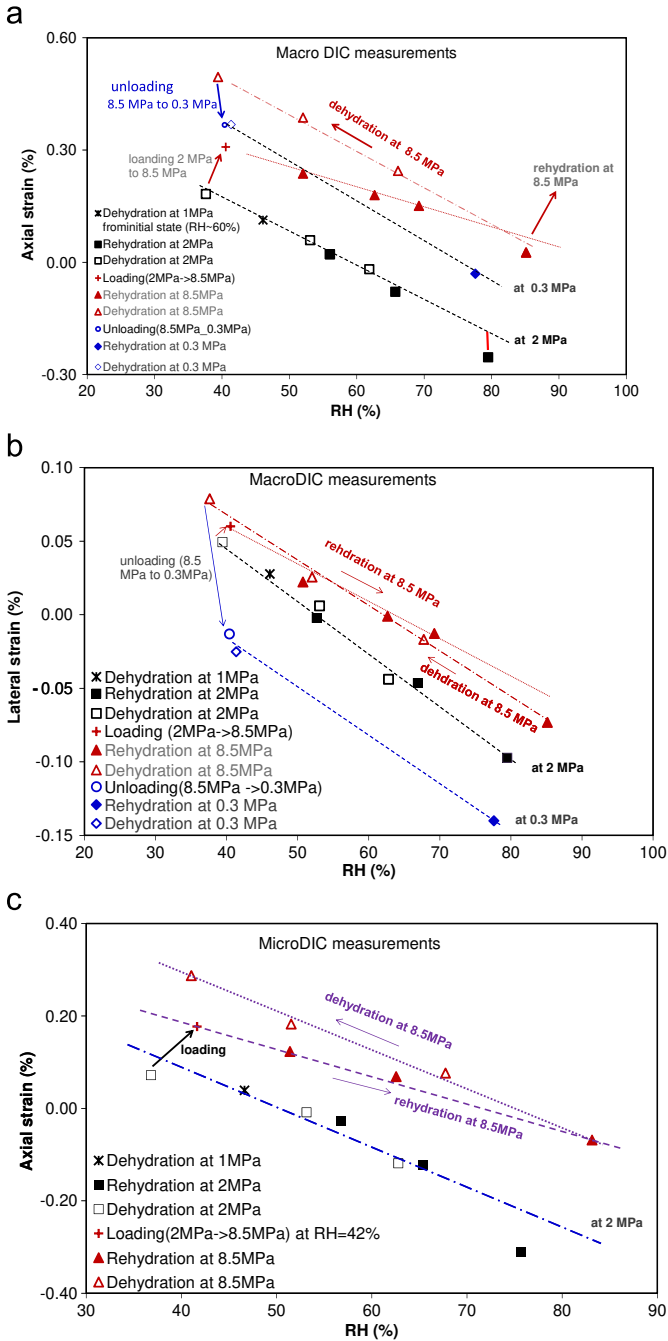


Fig. 9. (a) axial strain (MacroDIC), (b) lateral strain (MacroDIC) and (c) axial strain (MicroDIC), versus relative humidity at each moisture equilibrium state during three cycles of rehydration and dehydration at the different applied uniaxial stress (2 MPa, 8.5 MPa, 0.3 MPa).

This irreversible deformation at high applied stresses is also evident at the mesoscopic scale (millimetric gauge length) as shown in Fig. 9c.

When the applied stress is decreased to 0.3 MPa, the linear relation between the permanent axial strain and the relative humidity returns reversible with a slope very similar to the one at the applied stress of 2 MPa (Fig. 9).

In addition to this strong dependence of swelling strains with stress, a slight deviation from linearity is observed for the axial strain at the highest relative humidity (above 75%), with a deformation larger than the one expected from the linear relation. This is observed for all prescribed stresses. This offset of the strain

to the linear function could be related to the growth or propagation of micro cracks in the argillaceous matrix, as suggested by the work of Freissmuth [3], who observed by means of computed microtomography the opening of cracks when the relative humidity exceeded 80%. Such cracks could be induced by swelling pressures, which would induce local stresses that could surpass a local damage threshold. But other mechanisms such as non-linear swelling could also be considered as suggested by Wang et al. [30] who recently observed a similar nonlinear behaviour at higher moisture levels using DIC applied to environmental SEM imaging, but without any observation of microcracks.

The results presented above show evidences of the dependence of shrinkage and swelling on the applied stress: the material at high stress swells during rehydration less than at low stress. Contraction during dehydration seems however to be much less sensitive to applied stress. This dependency is also evident on the evolution of the ratio of the lateral strain (normal the stress direction) to the axial strain (in the stress direction) during hydration and dehydration (Fig. 10). The ratio is nearly constant (0.3) during hydration and dehydration at 2 MPa but is about 0.4 during rehydration and 0.25 during dehydration at 8.5 MPa. These ratios can be compared to those of Pham et al. [8], who have observed ratios closer to 1, corresponding to a lower anisotropy. The difference could be related to different initial anisotropy of the material. Another difficulty could be induced by a slight deviation of the orientation of the sample and of the strain gauges with respect to bedding. This problem is less critical with optical full field strain measurements than with classical strain gauge measurement as the whole in-plane strain tensor is measured and not only two components, we could check that lateral and axial strains indeed coincide with the principal strains.

A first interpretation of this dependence of swelling strains with axial stress could be related to the some dependence of the water content with stress: the higher stress would consolidate the material and change the pore size distribution, so as to reduce the absorption of water when humidity increases and induce a smaller dilation than at lower stress level. Conversely, during dehydration, the material would expel more water and exhibit a larger contraction than at lower stress level [6]. As it is very delicate to record water content during hydration under applied stress, the verification of such a dependence of water content with applied stress is left for further investigations.

A second interpretation could be related to viscous effects, since higher stress would increase more creep. But in this study, the highest stress is about 8.5 MPa, which was kept constant less than 3 months for different moisture levels. The creep rate of the MHM argillite is very low and has been measured to be

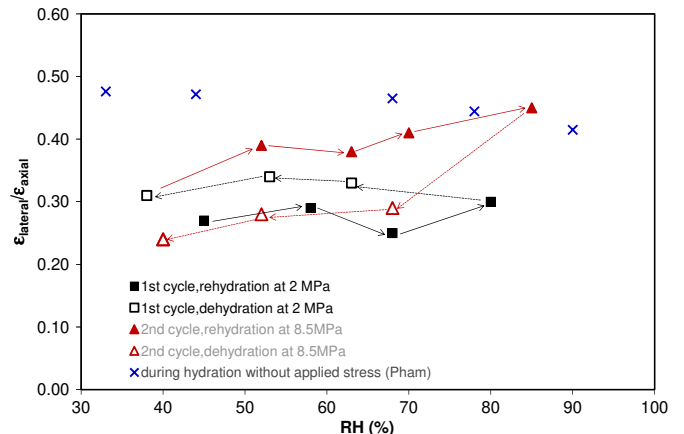


Fig. 10. Anisotropy coefficient versus relative humidity.

2.5×10^{-11} /s at 10 MPa axial stress and 75% relative humidity [31]. Under the present conditions, it should be even lower. Under such conditions, the expected creep strain would be less than 0.5×10^{-4} per month and thus very small with respect to the measured swelling strains. So creep is certainly not the principal reason for the low swelling at higher stress level. In addition, if creep would significantly contribute to deformation at 8.5 MPa, one would also observe higher compressive strains during dehydration than at lower stress, which is not the case.

A third interpretation could be related to the dependence of the elastic properties with water content. As shown in the next section, the axial elastic modulus indeed decreases with saturation. The applied constant stress induces thus an additional elastic contraction when humidity is changed, resulting in a reduced global swelling. This additional elastic strain can be evaluated to be less than 0.5×10^{-3} , when comparing hydration under 8.5 MPa with hydration at 2 MPa (decrease of Young's modulus from 9 to 6 GPa, with an additional stress of 6.5 MPa) and explains only one third of the reduction of the swelling strains. In addition, such a phenomenon cannot explain the irreversibility of the hydration/dehydration behaviour at high stress. It is highly likely that impurely elastic phenomena are activated during such combined hydromechanical loadings, the investigation of which is left for further experimental and theoretical investigations

5.2. Mechanical properties of the unsaturated argillaceous rocks

The strain versus stress curves are linear during the mechanical loading and unloading at both the macroscopic scale (cm) and the mesoscopic scale (mm) (Fig. 11a and b). Fig. 11a, which corresponds to a relative humidity of 69% during the first hydration cycle, also shows that the axial strain over the whole surface observed by MacroDIC is less than that determined from a local cracked zone (Fig. 15a), but it is larger than that determined from a local intact zone (Fig. 15b). An explanation is that the closure/opening of the cracks lead to a locally large deformation and the MacroDIC strain measurement represents the average response of the structural heterogeneity of the material.

Some delayed deformation is also observed after the mechanical loading or unloading. More precisely, after loading, the sample continues to contract when the applied stress of 8.5 MPa is kept constant about 15 min and the increase of the axial strain is about 7×10^{-5} . After unloading the sample continues to dilate when the applied stress of 2 MPa is kept constant for the same period and the decrease of the axial strain is 4×10^{-5} . At the end of these two cycles of mechanical loading and unloading, the irreversible strain is about 10^{-5} , and considered very small with respect to the evaluated strain induced by the stress change. This delayed behaviour of the material could be related to the primary creep of the matrix or the redistribution of water in the sample. Note that secondary creep (see previous section) is negligible at such time scales.

During the second cycle of dehydration and rehydration, when the axial stress is kept constant at 8.5 MPa and elastic moduli evaluated by reducing the stress, a similar linear relation between strain and stress is also at the stable hydric state (Fig. 11b). The irreversible strain is also of the order of 10^{-5} at the end of the mechanical unloading and loading cycles.

The axial Young's modulus (E) of the material at each moisture equilibrium state is determined from the unloading part of the stress-strain curve as sketched in Fig. 12a, b and this analysis is performed for all the 16 prescribed mechanical cycles. A linear relation between E and the relative humidity is found not only at the macro-scale (cm), but also at meso-scale (mm) as shown in Fig. 12a, over the investigated range of relative humidity, going from 39% to 85%. Note that the local moduli are evaluated

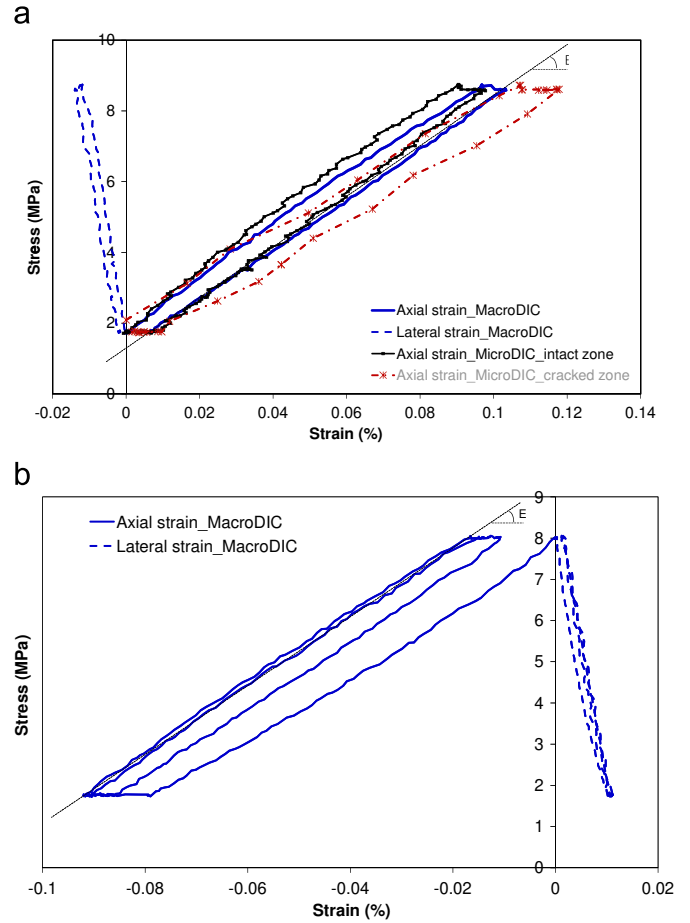


Fig. 11. Stress-strain curve at various scales during mechanical loading and unloading at the humidity of 68% (a: stage S4 during the first hydration and dehydration cycle; b: stage S13 during the second hydration and dehydration cycle).

assuming uniformity of the stress field, which is an approximation. The obtained values should not be considered as exact measures of local elastic moduli, but rather as a signature and a quantification of the heterogeneity of the response of the material during such macroscopically elastic loading cycles. Indeed, due to the structural heterogeneity, the values of the moduli obtained over the global surface are larger than those obtained from the local cracked zone. It is noticeable that the moduli at a given moisture level vary only very slightly from one hydration/dehydration cycle to the other (Fig. 12b). These variations of the moduli are much lower than those of Pham et al. [8]. The difference is probably related to the initial states of the samples and to the hydration conditions. The samples used in the study of Pham et al. were probably more damaged at their initial state and, more importantly, were hydrated/dehydrated without any confining axial stress, so that their damage level probably increased during the hydration/dehydration cycles. Moreover in the analysis of Pham et al., each elastic modulus measurement was obtained with a different sample, thus generating some possible randomness, even though they were extracted from the same core plug. A definitive advantage of the present study is that all measurement (swelling strains and elastic moduli) are obtained from the same sample, so that the sole effect of the hydration history is investigated, without any additional randomness linked to microstructure fluctuations. The obtained moduli at the macroscale in this study present some clear consistency with those measured at the mesoscale by Ibrahim, who characterised

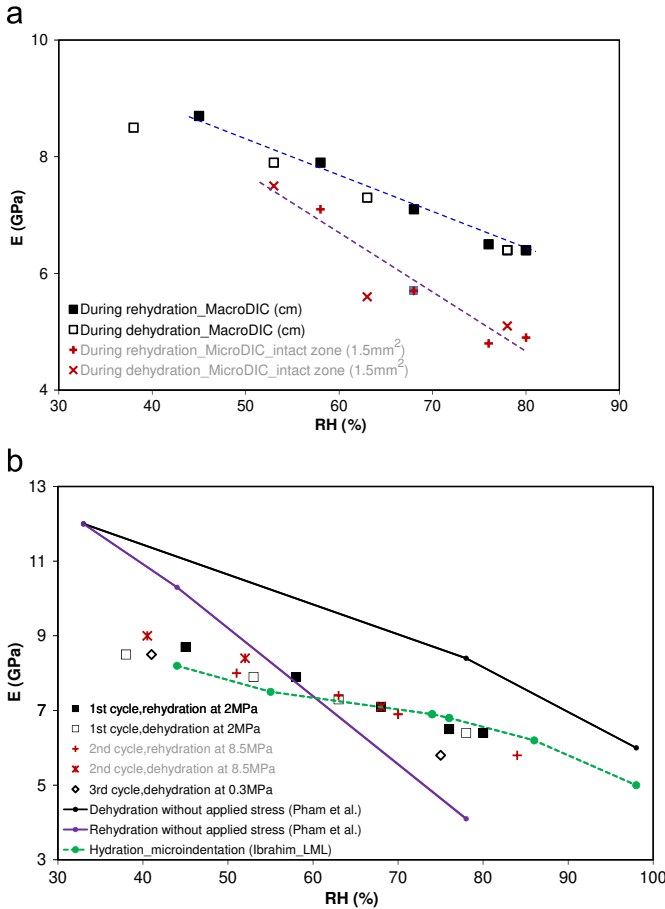


Fig. 12. (a) Moduli versus relative humidity evaluated at macroscale and microscale during the first cycle of rehydration and dehydration; (b) moduli at macroscale versus relative humidity for the whole test and comparison with data from literature.

the dependence of the elasticity with the relative humidity of the same material by using a micro-indentation technique which explores elastic properties over domains millimetric in size [32]. But the linear dependence of elastic moduli with relative humidity is much clearer in our study, probably because, again, a single sample has been used and fluctuations due to microstructure variability from one sample to the other are avoided.

Finally, the Poisson's ratio remains, as a first approximation, constant during the various cycles of rehydration and dehydration (Fig. 13). The results are in good agreement with those of Pham et al. in the same range of relative humidity. One may notice that the Poisson's ratio measured during the rehydration/dehydration cycle at 8.5 MPa is slightly lower than during the cycles at lower axial stress. This result should however to be taken with care, as such small differences in Poisson's ratio correspond to differences in transverse strains of the order of 3×10^{-5} , which is near the accuracy limit of the measurements.

5.3. Heterogeneity

The heterogeneous response of the material related to microstructural and mineralogical composition can be characterised by the full-field strain maps at various scales provided by the DIC technique. All strain maps confirm that the argillaceous rocks contract during dehydration and dilate during rehydration rather uniformly both at the macroscale and the mesoscale (mm) (Figs. 14 and 15). These strain maps show however different responses near pre-existing mesocracks (with a typical extension

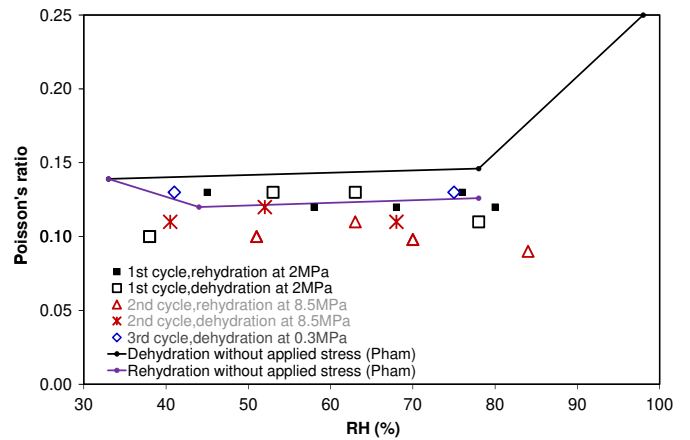


Fig. 13. Poisson's ratio evaluated at macroscale (cm) versus relative humidity.

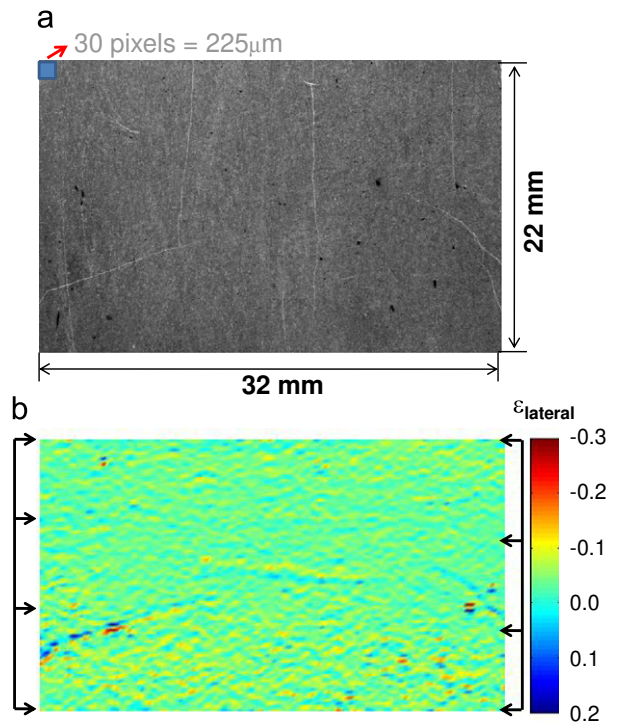


Fig. 14. Lateral strain map of the whole surface when the relative humidity increases from 41% to 71% at 8.5 MPa.

of several millimetres), the behaviour of which depends in addition on their direction relative to the applied stress. The cracks presenting a small angle with respect to the applied stress direction close during rehydration (Fig. 14b) and open during dehydration at 8.5 MPa, while the cracks nearly perpendicular to the applied stress (i.e. nearly parallel to bedding) exhibit a hydric response similar to that of the other undamaged parts of the sample during the hydration cycles at 2 MPa (Fig. 15c and d) or 8.5 MPa: they do not contribute to the overall swelling strains. This contrasted response to relative humidity changes of the cracks can be explained by the fact that the swelling of the clayey matrix can close mesocracks inclined to the applied stress, which are still slightly open in the sample, while it influences much less the other cracks perpendicular to the applied stress, which have been totally closed by the prior mechanical load.

The strain maps show evidences of the slight heterogeneous deformation at the scale of a few hundred micrometres during

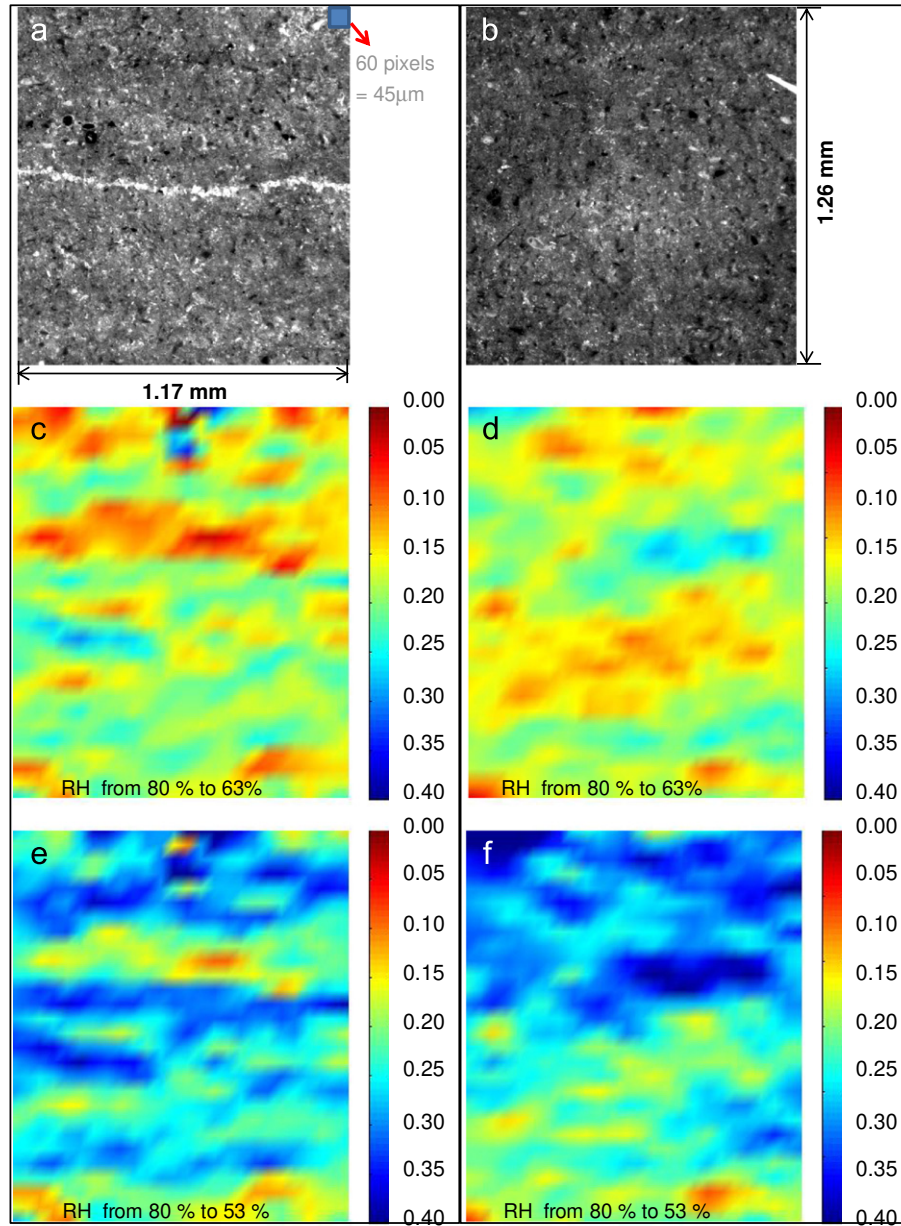


Fig. 15. Microstructure and axial strain map of the local cracked zone ($1.1 \times 1.2 \text{ mm}^2$; a,c,e) and of the intact zone ($1.1 \times 1.2 \text{ mm}^2$; b,d,f) when the relative humidity decreases from 80% to 63% (c,d) and from 80% to 53% (e,f) at 2 MPa axial stress.

dehydration/hydration loading as shown in Fig. 15c–f, which present the strain maps of two different zones at the mesoscopic scale ($1.1 \times 1.2 \text{ mm}^2$) during two different dehydration steps. This strain heterogeneity can be related to the mineralogical composition which can be qualitatively guessed from the grey levels of the corresponding images from the optical microscope (Fig. 15b). The comparison of the results at the macroscopic scale (cm) and at the microscopic scale ($100 \mu\text{m}$) shows that the size of representative volume element (RVE) is probably of the order of a few hundred micrometres, which is consistent with the estimate of the RVE size relative the mechanical deformation presented in Ref. [5].

6. Summary and Conclusions

In order to investigate the behaviour of argillaceous rocks under coupled hydro-mechanical conditions, a specific optical setup has been developed to observe argillaceous rocks submitted to

combined moisture-mechanical loading conditions and measure the induced low strains at macro and microscale. Thanks to various optimisation procedures, the accuracy of this system has been improved and is better than 10^{-5} at macroscale (3 mm gauge length) and 10^{-4} at microscale (about $100 \mu\text{m}$ gauge length).

Using this optical setup, a complex test consisting of three cycles of rehydration and dehydration from 39% to 85% at different stress levels (2, 8.5 and 0.3 MPa) was performed on a single COx argillaceous rock sample. The results confirm that this argillaceous rock contracts during dehydration and swells during rehydration. A linear relation is found between the deformation and the relative humidity when the later is less than 75%. It is reversible during hydration and dehydration at low stresses (0.3 MPa, 2 MPa) and is irreversible at 8.5 MPa. The high applied axial stress limits the swelling of the material during rehydration but has much less effect on shrinkage. This observed behaviour does not have a simple interpretation and is probably the signature of complex nonlinear hydromechanical couplings.

The strain induced by the rehydration or dehydration is relatively homogeneous at the mesoscopic scale (mm) and heterogeneous at the sub-mesoscopic scale (a few hundred micrometres), because of the mineralogical composition which is heterogeneous at this scale. The preexistent cracks perpendicular to the applied stress are closed during the mechanical loading and do not move during the hydration/dehydration cycles at constant stress. These cracks do however open or close when the stress is modified and contribute to a small heterogeneity in the sample response to mechanical load. Cracks nearly parallel to the applied stress are not constrained by the axial load, and move during both hydric and mechanical changes of the loading conditions.

A clearly linear relation between strain and stress is observed for the low stress amplitudes considered in this study (below 8.5 MPa) and a linear dependence of the elastic moduli on the relative humidity is evident over the considered range of relative humidity (39%–85%), with lower moduli at higher water content. The axial modulus and the Poisson's ratio measured at a given moisture level almost do not evolve during the complex hydric/mechanical loading history considered in this study. Some delayed response of the sample after mechanical loading or unloading has been observed, with strain amplitudes of the order of 10^{-5} . The corresponding strain rates tend to very low values after a few minutes.

All the presented results have been obtained with a single sample tested during almost one year. Such a procedure allows us to investigate accurately the dependence of mechanical properties with moisture content. Indeed, unlike in more classical investigations, for which results obtained with different samples need to be compared, the fluctuations linked to the variability of the sample composition are avoided.

Acknowledgements

The authors gratefully acknowledge ANDRA for financial support and for providing core samples. The microstructure image presented in Section 3 was obtained with the environmental SEM FEI Quanta 600 which has been acquired with the financial support of Region Île de France (SESAME 2004 program), CNRS and École Polytechnique. The authors would like to thank the reviewers and the editors for their constructive comments.

References

- [1] Yang DS, Billote J, Su K. Characterization of the hydromechanical behaviour of argillaceous rocks with effective gas permeability under deviatoric stress. *Eng Geol* 2010;114(3–4):116–122.
- [2] Valès F, Nguyen MD, Gharbi H, Rejeb A. Experimental study of the influence of the degree of saturation on physical and mechanical properties in Tournemire shale (France). *Appl Clay Sci* 2004;26:197–207.
- [3] Freissmuth H. Influence de l'eau sur le comportement mécanique des roches argileuses [Influence of water on the mechanical behavior of argillaceous rocks]. PhD thesis. École Nationale Supérieure des Mines de Paris: 2002. 122 p.
- [4] Gaucher E, Robelin C, Matray JM, Negral G, Gros Y, Heitz JF, et al. ANDRA underground research laboratory: interpretation of the mineralogical and geochemical data acquired in the Callovian–Oxfordian formation by investigative drilling. *Phys Chem Earth* 2004;29(1):55–77.
- [5] Bornert M, Valès F, Gharbi H, Nguyen MD. Multiscale full-field strain measurements for micromechanical investigations of the hydromechanical behavior of clayey rocks. *Strain* 2010;46:33–46.
- [6] Gasc-Barbier M. Etude des mécanismes de déformation de roches argileuses profondes: Apport de la microstructure et des analyses pétrophysiques. PhD dissertation. Université Pierre et Marie Curie: 2004. 214 p.
- [7] Chiarelli A, Shao J, Hoteit N. Modeling of elastoplastic damage behavior of a claystone. *Int J Plast* 2003;19:23–45.
- [8] Pham QT, Valès F, Malinsky L, Nguyen MD, Gharbi H. Effects of desaturation–resaturation on mudstone. *Phys Chem Earth* 2007;32:646–655.
- [9] Valès F. Modes de déformation et d'endommagement de roches argileuses profondes sous sollicitations hydro-mécaniques. PhD dissertation. Ecole Polytechnique: 2008. 356 p.
- [10] Jia Y, Bian HB, Su K, Kondo D, Shao JF. Elastoplastic damage modeling of desaturation and resaturation in argillites. *Int J Numer Anal Meth Geomech* 2010;34(2):187–220.
- [11] Zhang C, Rothfuchs T. Experimental study of the hydro-mechanical behaviour of the Callovo-Oxfordian argillite. *Appl Clay Sci* 2004;26:325–336.
- [12] Yang DS, Bornert M, Chanchole S, Gharbi H, Valli P. Optimized optical setup for DIC in rock mechanics. *Eur Phys J* 2010. <http://dx.doi.org/10.1051/epjconf/20100622019>.
- [13] Chu TC, Ranson WF, Sutton MA, Peters WH. Applications of digital-image-correlation techniques to experimental mechanics. *Exp Mech* 1985;25(3):232–244.
- [14] Sutton MA, Orteu JJ, Schreier H. Image correlation for shape, motion and deformation measurements. Berlin: Springer; 2009.
- [15] Bornert M, Orteu JJ, Roux S. Corrélation d'Images. In: Grédiac M, Hild F, editors. Mesures de champs et identification en mécanique des solides. Paris: Hermes Science Publications; 2011.
- [16] Dautria J, Bornert M, Gland N, Dimanov A, Raphanel J. Localized deformation induced by heterogeneities in porous carbonate analysed by multi-scale digital image correlation. *Tectonophysics* 2011;503(1–2):100–116.
- [17] Nguyen TL, Hall SA, Vacher P, Viggiani G. Fracture mechanisms in soft rock: Identification and quantification of evolving displacement discontinuities by extended digital image correlation. *Tectonophysics* 2011;503(1–2):117–128.
- [18] Lenoir N, Bornert M, Desrues J, Bésuelle P, Viggiani G. Volumetric digital image correlation applied to X-ray micro tomography images from triaxial compression tests on argillaceous rock. *Strain* 2007;43(3):193–205.
- [19] Schreier HW, Sutton MA. Systematic errors in digital image correlation due to undermatched subset shape functions. *Exp Mech* 2002;42(3):303–310.
- [20] Wang YQ, Sutton MA, Bruck HA, Schreier HW. Quantitative error assessment in pattern matching: effects of intensity pattern noise, interpolation, strain and image contrast on motion measurements. *Strain* 2009;45:160–178.
- [21] Sutton MA, Yan JH, Tiwari V, Schreier H, Orteu JJ. The effect of out-of-plane motion on 2D and 3D digital image correlation measurements. *Opt Laser Eng* 2008;46:746–757.
- [22] Allais L, Bornert M, Bretheau T, Caldemaison D. Experimental characterization of the local strain field in a heterogeneous elastoplastic materials. *Acta Metall Mater* 1994;42:3865–3880.
- [23] Escoffier S. Caractérisation expérimentale du comportement hydromécanique des argilites de Meuse/Haute-Marne. PhD thesis. INPL: 2002. 242 p.
- [24] Homand F, Giraud A, Escoffier S, et al. Permeability determination of a deep argillite in saturated and partially saturated conditions. *Int J Heat Mass Transfer* 2004;47:3517–3531.
- [25] Delage P, Howat MD, Cui YJ. The relation between suction and swelling properties in a heavily compacted unsaturated clay. *Eng Geol* 1998;50:31–48.
- [26] Young A, Low P. Osmosis in argillaceous rocks. *Bull Am Assoc Pet Geol* 1965;49(7):1004–1008.
- [27] Santarelli F, Forsans T, et al. Shale testing and capillary phenomena. *Int J Rock Mech Min Sci* 1994;31(5):411–427.
- [28] Stepkowska E. Aspects of the clay electrolyte water system with special reference to geotechnical properties of clays. *Eng Geol* 1990;28:249–268.
- [29] Saiyou N, Tessier D, Hicher PY. Experimental study of swelling in unsaturated compacted clays. *Clay Miner* 2004;39:469479.
- [30] Wang LL, Yang DS, Eva H, Bornert M, Chanchole S, Halphen B, et al. Microscale experimental investigation of deformation of argillaceous rocks under hydric loads. *Appl Clay Sci* in press.
- [31] Yang DS, Bornert M, Chanchole S. Experimental investigation of the delayed behaviour of unsaturated argillaceous rocks by means of Digital Image Correlation techniques. *Appl Clay Sci* 2011;54:53–62.
- [32] Ibrahim N. Caractérisation des propriétés mécaniques des géomatériaux par technique de micro indentation [Characterization of mechanical properties of geomaterials by the technique of microndentation]. PhD thesis. Université des Sciences et Technologies de Lille: 2008. 135 p.